Noise gradiometry and wavefield reconstruction inversion

Biondo Biondi

ABSTRACT

Noise gradiometry is a special case of wavefield reconstruction inversion when the propagating wavefield is recorded at every point within the domain of interest. In this favorable, but typically unrealistic, case the method provides accurate and high-resolution estimates of seismic velocities. It can recover both the short and long wavelengths of unknown velocity perturbations. However, if the data are irregularly sampled, or the recording is limited to the boundary of the domain (surface), the quality of the velocity estimate depends on the quality of the wavefield reconstruction. A simple synthetic-data example in which the wavefield is randomly subsampled by a factor of two shows the challenges encountered by the method by poor reconstruction of the wavefield.

INTRODUCTION

In a recent report de Ridder and Biondi (2014) introduced the idea of "chaotic gradiometry" (then renamed noise gradiometry (NG) in de Ridder and Biondi (2015)) to estimate wave-propagation velocity from surface-waves noise recorded by dense arrays. The method is attractive because it requires much shorter recordings to converge towards good velocity estimates than conventional methods based on seismic interferometry followed by tomography (de Ridder, 2014), and is much less computationally expensive than conventional methods. The major limitation of the new method is that it requires a dense and fairly regular array. Furthermore, it assumes that surface wave-propagation is accurately modeled by the 2D scalar constant density wave-equation defined at the Earth's surface, therefore limiting its applicability for imaging a highly heterogeneous subsurface using surface waves. To overcome these limitations, I explore the connections of NG with wavefield reconstruction inversion (WRI) as introduced by van Leeuwen and Herrmann (2013). WRI attempts to image acoustic properties (e.g. velocity) in a volume by solving two combined estimation problems: 1) reconstruct the complete wavefield that propagated in the volume, and 2) estimate the acoustic parameters from the reconstructed wavefield. Indeed, noise gradiometry can be seen as a special case of WRI when the wavefield is fully recorded, and therefore it does not need to be reconstructed before estimating the wave-equation parameters.

The potential advantages of applying WRI concepts to generalize noise gradiometry are that: 1) data recorded from irregular arrays may be used, and 2) near-surface

heterogeneity can be imaged directly by using the appropriate 3D elastic wave equation. Beyond passive-seismic imaging, I am interested to investigate whether the method could be applied to image near-surface heterogeneity from surface waves recorded by modern single-sensors dense arrays during active experiments on land. Curtis and Robertsson (2002) presented related ideas applied to the suppression of surface-waves in land data recorded using novel acquisition geometries.

The results of my limited numerical experiments confirm that NG, and thus WRI, can be used to estimate propagation velocity very accurately from data recorded by a regularly sampled array. However, my attempts to apply the method to irregularly sampled data have not yielded yet as encouraging results as the ones from regularly sampled data. I attribute these results to the failure of the reconstruction step, as I implemented it, to provide a sufficiently accurate wavefield to the velocity estimation step.

FROM CHAOTIC GRADIOMETRY TO WAVEFIELD RECONSTRUCTION INVERSION

The main idea behind noise gradiometry is very simple. If we know the wavefield at every location in a volume (or surface in 2D), the velocity (or slowness) at every point in the domain can be estimated as the ratio between the second time derivatives and the Laplacian of this wavefield. The estimates of this ratio might be noisy because of numerical approximations in the computation of the time and spatial derivatives and because of noise in the data. However, if we have sufficiently long recordings, and can assume that velocity is stationary in time, we can take advantage of the redundant information over the time axis to intelligently "average " the quantities measured from the data over time and derive a stable estimator (de Ridder and Biondi, 2015).

A little more formally, we can start from the scalar acoustic wave equation without sources; that is,

$$s\left(\vec{x}\right)^2 \frac{\partial^2 p\left(t,\vec{x}\right)}{\partial t^2} - \nabla^2 p\left(t,\vec{x}\right) = 0, \tag{1}$$

where p is the pressure field defined at time t and position $\vec{x}$, and s is the slowness function, that we assume is heterogeneous in space but stationary in time. Ignoring the source term in the equation is reasonable in passive imaging when we image microseism energy generated far away from the recording array. When the data, $d\left(t,\vec{x}\right)$ were generated by active sources placed within the recording array, the source term could be easily introduced in 1.

If the recorded data, $d\left(t,\vec{x}\right)$, sample the wavefield at every point in the domain, the slowness-squared function can be estimated at each point in the domain by

$$s\left(\vec{x}\right)^2 = \left\langle \frac{\nabla^2 d\left(t,\vec{x}\right)}{\frac{\partial^2 d(t,\vec{x})}{\partial t^2}} \right\rangle, \tag{2}$$

where the symbols $\langle\ \rangle$ indicate an appropriate average in time to stabilize the velocity estimate.

If we discretize the wave equation in time and space, equation 1 can be written as:

$$\mathbf{A}\left(\mathbf{s^2}\right)\mathbf{p}=0, \tag{3}$$

where $\mathbf{A}$ is the discretized wave-equation operator, $\mathbf{s^2}$ is the vector representing the slowness-squared uniformly distributed in space, and $\mathbf{p}$ is the pressure field vector.

Equation 3 immediately suggests an optimization-based approach to estimate the slowness-square vector that is equivalent to NG; we can estimate $\mathbf{s^2}$ by solving the following minimization problem

$$\min_{\mathbf{s^2}} J_{\mathrm{CG}}\left(\mathbf{s^2}\right), \tag{4}$$

with

$$J_{\mathrm{CG}}\left(\mathbf{s^2}\right)=\left\|\mathbf{A}\left(\mathbf{s^2}\right)\mathbf{d}\right\|_2^2, \tag{5}$$

where $\mathbf{d}$ is the vector of recorded data that we assume have been recorded everywhere in the domain, or at least sampled densely enough not to be spatially aliased. The optimization problem formulated in 5 can be solved iteratively with a conjugate-gradient algorithm. Since this solution is iterative and not direct, like the one in equation 2, I will refer to this method as iterative NG (ING).

Wavefield Reconstruction Inversion

Wavefield Reconstruction Inversion was introduced as a (potentially more robust) alternative to conventional full waveform inversion (FWI) (van Leeuwen and Herrmann, 2013; van Leeuwen T. et al., 2014). In WRI the velocity estimation problem is posed as the following minimization problem:

$$\min_{\mathbf{p},\mathbf{s^2}} J_{\mathrm{WRI}}\left(\mathbf{p},\mathbf{s^2}\right), \tag{6}$$

with the objective function that is a function of both the slowness-squared vector $\mathbf{s^2}$ and the wavefield $\mathbf{p}$, and is defined as

$$J_{\mathrm{WRI}}\left(\mathbf{p},\mathbf{s^2}\right)=\|\mathbf{K}\mathbf{p}-\mathbf{d}\|_2^2+\lambda\left\|\mathbf{A}\left(\mathbf{s^2}\right)\mathbf{p}\right\|_2^2, \tag{7}$$

where $\mathbf{K}$ is a data-sampling operator. This minimization problem can be solved, as suggested by van Leeuwen T. et al. (2014), by the following procedure. We first minimize both terms in equation 7 as a function of $\mathbf{p}$, given an initial estimate of slowness-squared vector ($\mathbf{s_o^2}$), and obtain an estimated wavefield $\widetilde{\mathbf{p}}$. We can then update $\mathbf{s^2}$ by minimizing the second term in equation 7 with $\widetilde{\mathbf{p}}$ in place of $\mathbf{p}$. If needed, we could iterate on this "alternating directions" algorithm.

In the special case when we record the data at every point in the domain of interest (i.e. $\mathbf{K} \equiv \mathbf{I}$), we set $\mathbf{p} = \mathbf{d}$, and the objective function simplifies into the iterative NG objective function 5.

My numerical experiments indicates that the reconstructed wavefield obtained by the first step of the process may be severely degraded by short-wavelength noise. I therefore added a regularization term to the objective function in 7 and minimized the following regularized objective function:

$$J_{\widehat{\text{WRI}}}\left(\mathbf{p}, \mathbf{s^2}\right) = \|\mathbf{K}\mathbf{p} - \mathbf{d}\|_2^2 + \lambda \left\|\mathbf{A}\left(\mathbf{s^2}\right)\mathbf{p}\right\|_2^2 + \epsilon \left\|\mathbf{\Delta}\mathbf{s^2}\right\|_2^2, \tag{8}$$

where $\mathbf{\Delta}$ is a discretized version of the Laplacian operator.

It is important to notice that if we minimize the WRI objective function using gradient-based optimization methods we only need to apply the operator $\mathbf{A}$ and its Fréchet-derivatives operator with respect to slowness-squared ($\mathbf{G_{s^2}}$); these operators act locally on the wavefields and slowness-squared. The computational cost of applying $\mathbf{A}$ and $\mathbf{G_{s^2}}$ is much lower than the one associated with the computation of gradients in conventional FWI because WRI gradients do not require wavefield propagation. Therefore, for time-domain solutions we do not have to worry about imposing a sufficiently small time-stepping interval to ensure stability as we must do when propagating wavefields using efficient explicit finite-differences propagators.

The field-data results presented in de Ridder and Biondi (2015), and the results of the numerical experiments presented in the next sections, indicate that NG is quite robust with respect to arbitrary wavefield blending; that is, when the data are generated by sources overlapping in time. The reason for this attractive property is not obvious because the gradient with respect to the model parameter contains crosscorrelations between wavefields, much like the FWI gradients. Consequently, the gradient contains cross-terms between the blended wavefields. The reasons why the results shown in this paper seem to demonstrate that the cross-terms in the gradient do not derail the inversion deserve further analysis. One intuitive explanation might be the fact that the Laplacian and the second time derivative in equation 2 are linear with respect to the wavefield, although the ratio is not.

SYNTHETIC DATA EXAMPLES

I tested the effectiveness of ING and WRI to estimate both short-wavelength and long-wavelength velocity perturbations, with and without blended sources. In the first set of experiments I assumed that the data were recorded at every point within the computational grid, and then solved the optimization problem described in 4. In the last experiment I randomly subsampled the recorded wavefield by a factor of two in space, and estimated both the full wavefield and the velocity perturbations by minimizing the objective function 8.

In all my experiments I used the same constant-density wave-equation for both modeling and inversion. Furthermore, the derivative operators discretization was also

the same for both the modeling and inversion phases. Therefore, I plead guilty of inverse crime.

Estimating short-wavelength velocity perturbations

Figure 1 shows the model used for testing the capability of ING to estimate short-wavelength perturbations from reflections and diffractions. It shows the whole computational domain, whereas Figure 2 shows the subset where I assume to have the data recorded at every point within the domain.

Figure 3a shows a snapshot of the data generated by one source located at x=3.5 km and y=1.5 km; that is, outside the window where the data were recorded. Figure 3b shows the data recorded when three sources (including the one corresponding to the data shown in Figure 3) were active; all sources were located outside the recording array.

Figure 4 shows the results of the ING estimation obtained by a few iterations of a conjugate-gradient algorithm applied to the optimization problem described in 4. The panel on the left (Figure 4a) was obtained by inverting the data recorded when only one source was active (Figure 3a), whereas the panel on the right (Figure 4b) was obtained by inverting the data recorded when three source were active (Figure 3b). Both inversion results are accurate and high resolution.

Estimating long-wavelength velocity perturbations

Figure 5 shows the model used for testing the ability of the methods to estimate long-wavelength perturbations by exploiting the bending and distortion of the propagating wavefields. Figure 5 shows the velocity model in the area where the data are recorded.

Figure 6a shows a snapshot of the data recorded corresponding to one source located at x=3.5 km and y=1.5 km; that is, outside the window where the data are recorded. Figure 6b shows the data recorded when three sources (including the one corresponding to the data shown in Figure 6a) were active; all of them located outside the recording array. Notice that the low-velocity anomaly is sufficiently strong to cause triplications in the propagating wavefields. The snapshots shown in Figure 6 is taken just after one of the wavefields went through a caustic.

Figure 7 shows the result of the ING estimation obtained by a conjugate gradient algorithm solving the optimization problem described in 4 and applied to data generated by three blended sources. Figure 7a shows the result after one iteration, whereas Figure 7b shows the results after 10 iterations, when the optimization had reached full convergence. The presence of caustics in the recorded wavefield creates artifacts in the first gradient, however the method overcomes this challenge, and converges to an accurate solution after only a few iterations. The artifacts related to the caustics

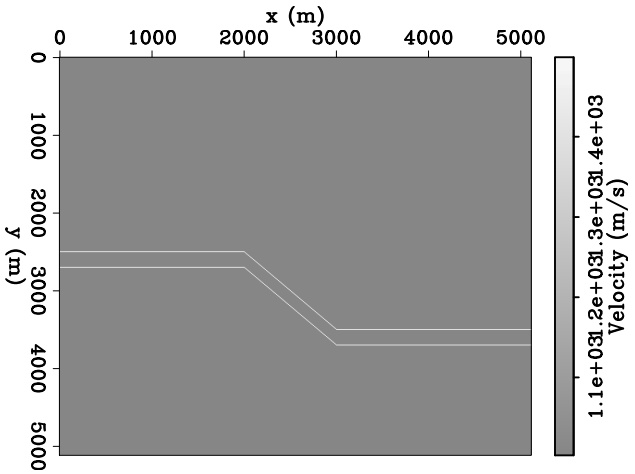

Figure 1: Model used to test the capability of ING to estimate short-wavelength perturbations from reflections and diffractions. [**ER**]

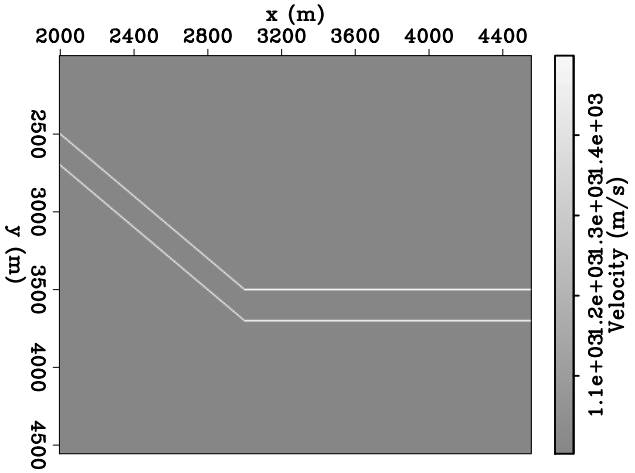

Figure 2: Subset of the model shown in Figure 1 where the data were recorded. [**ER**]

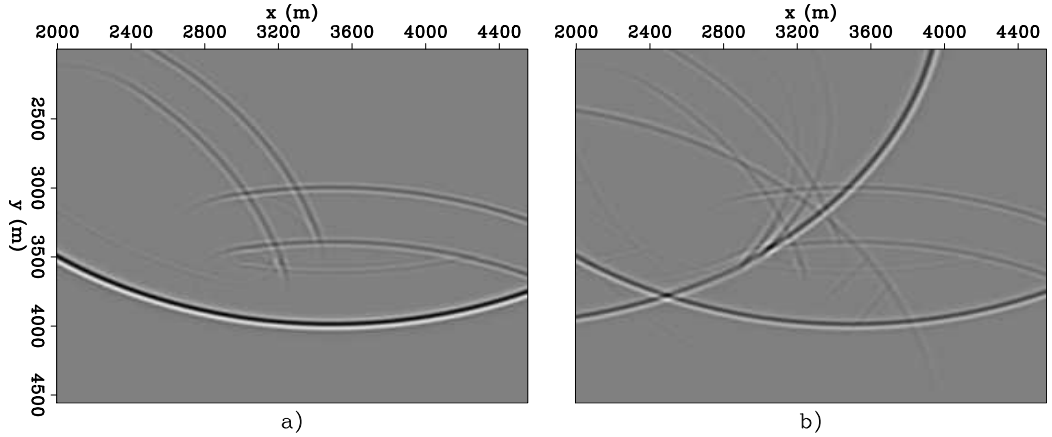

Figure 3: Snapshots taken at t=2.5 s of wavefields propagating through the model shown in Figure 1 and generated with: a) one source, and b) three blended sources. All sources are located outside the recording array. [**ER**]

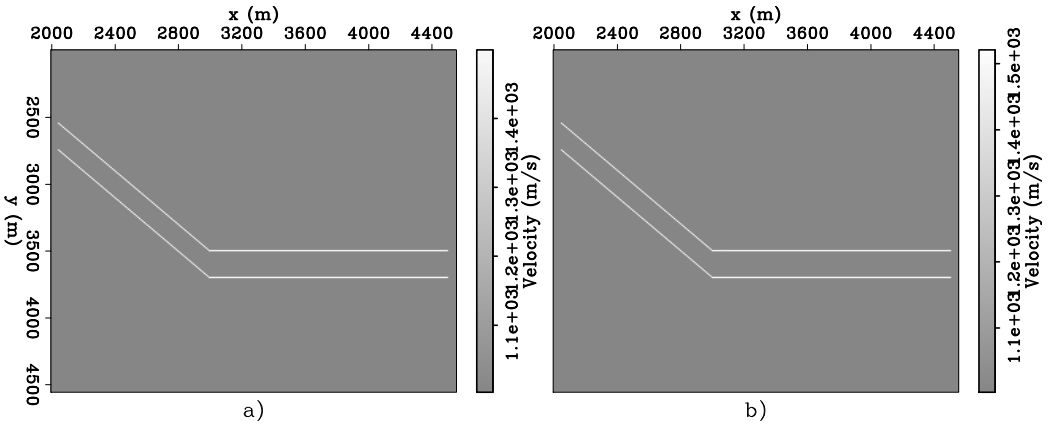

Figure 4: Inversion results obtained by a few iterations of a conjugate-gradient algorithm applied to the optimization problem described in 4 with data generated using: a) one source, and b) three blended sources. [**ER**]

are almost completely removed and the estimated velocity is almost identical to the one in the model used to record the data.

WRI applied to irregularly sampled data

The previous examples assumed that the wavefields were completely and regularly sampled by the recorded data. Therefore, the wavefield reconstruction step of WRI was not required and simple ING could be used to estimate velocity perturbations. The next example shows the result of applying both steps of the WRI alternating-directions algorithm outlined above to an irregularly sampled dataset. First, I minimized objective function 8 to estimate a fully-sampled wavefield vector $\widetilde{\mathbf{p}}$, assuming that $\mathbf{s_o^2}$ was uniform and corresponding to the unperturbed velocity of 1 km/s. The starting model for this step was the original subsampled data interpolated on the uniform grid by applying a simple bi-linear interpolator. Second, I applied the second step of WRI to $\widetilde{\mathbf{p}}$ for estimating velocity perturbations.

Figure 8a shows the mask ($\mathbf{K}$ in equation 8) that I used to randomly subsample the wavefield generated by three sources and propagating through the Gaussian anomaly shown in Figure 5. Figure 8b shows a time snapshot of the subsampled wavefield; it compares with Figure 6b that shows the snapshot at the same time, but before subsampling.

Figure 9a shows the estimated velocity model after 10 iterations of conjugate gradient applied to the reconstructed wavefield $\widetilde{\mathbf{p}}$. This result is dominated by artifacts related to the caustics in the wavefield and by short-wavelength noise. These artifacts could not be attenuated even by using a large weight ϵ to the regularization term in 8. Unfortunately, letting the conjugate-gradient optimization run for more iterations did not change the final results. As it can be surmised from the residual curve shown in

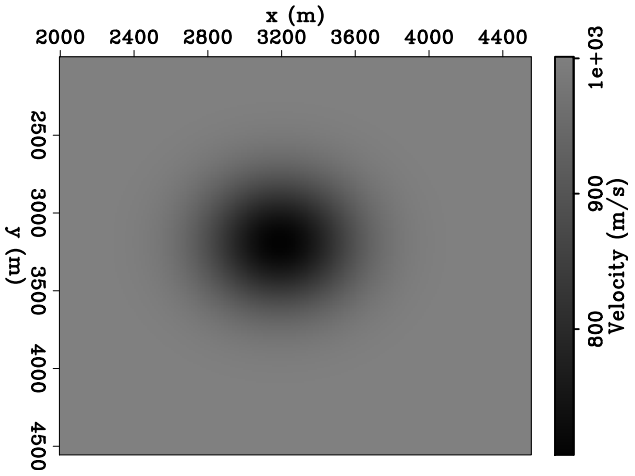

Figure 5: Model used to test the capability of the methods to estimate long-wavelength perturbations by exploiting the bending and distortion of the propagating wavefields. [**ER**]

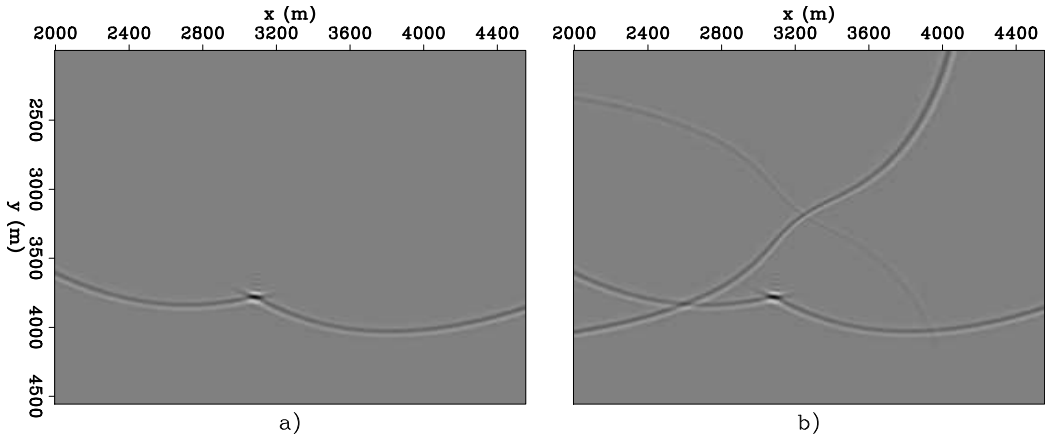

Figure 6: Snapshots taken at t=2.6 s of wavefields propagating through the model shown in Figure 5 and generated with: a) one source, and b) three blended sources. All sources are located outside the recording array. [**ER**]

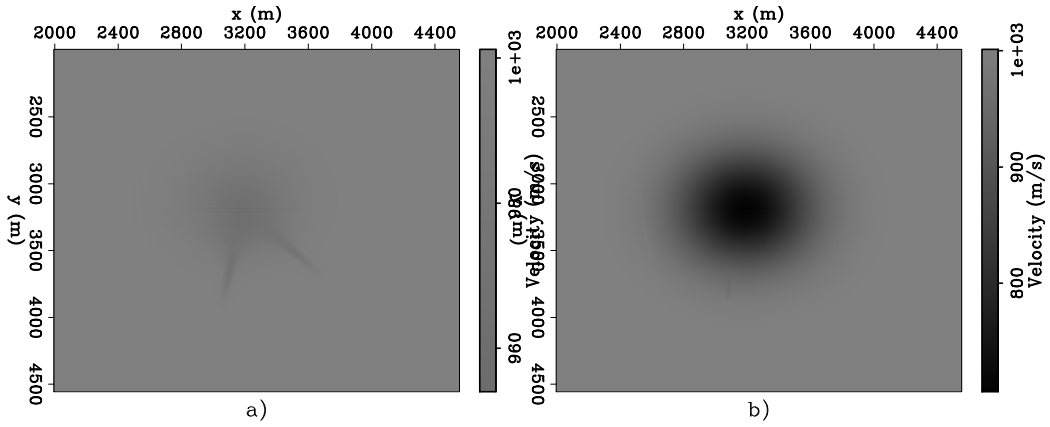

Figure 7: Results of ING estimation from data generated by three blended sources (Figure 6b): a) after one iteration, and b) after 10 iterations. [**ER**]

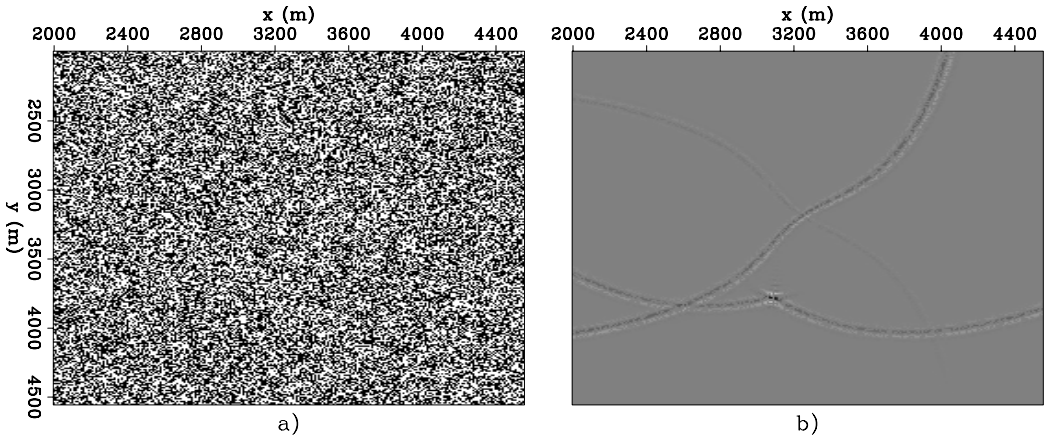

Figure 8: Mask used to subsample the wavefield before recording (panel a), and snapshot of recorded data (panel b). [**ER**]

Figure 9b, the inversion had reached a high plateau, and could not advance further.

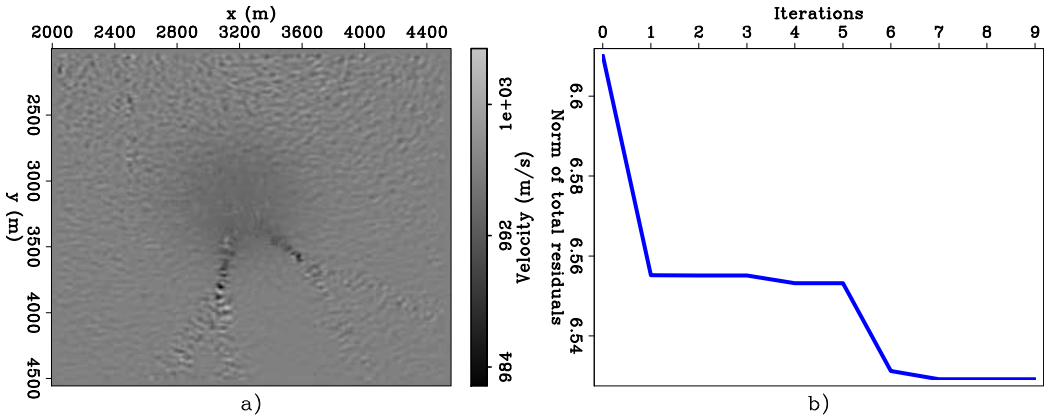

Figure 9: Inversion results after 10 iterations of the velocity-update step of WRI (panel a), and corresponding residual curve as a function of iterations (panel b). Notice that the vertical axis in panel b) does not start at the origin. [**CR**]

CONCLUSIONS

Wavefield reconstruction inversion (WRI) provides a natural framework for broadening the range of problems that can be tackled by noise gradiometry (NG). To achieve this goal, NG must at least be able to handle irregularly sampled datasets. Even more appealing, and challenging, would be to extend the method to problems where the degree of near-surface heterogeneity requires surface-waves to be accurately modeled by the 3D elastic wave equation instead of being approximately modeled by a 2D acoustic wave equation.

Unfortunately, when I applied WRI to a synthetic dataset randomly subsampled by a factor of two, the methods failed to yield good estimates of velocity perturbations. In contrast, when I applied ING to the same data, but without subsampling, the results were excellent. Therefore, I conclude that the problem is with the wavefield-reconstruction step of the two-step process employed in WRI.

The difficulties I encountered might be overcome by using a better implementation of the wavefield-reconstruction step than the simple minded I employed, or they may be caused by a fundamental problem with WRI. van Leeuwen T. et al. (2014) presented results obtained by solving the problem in the frequency domain, ad thus they were able to apply a Gauss-Newton algorithm instead of a conjugate-gradient algorithm to minimize the objective function.

ACKNOWLEDGMENTS

The understanding that noise gradiometry is related to wavefield reconstruction inversion surfaced during conversations with Sjoerd de Ridder when he was visiting SEP in the summer of 2014.

REFERENCES

Curtis, A. and J. O. A. Robertsson, 2002, Volumetric wavefield recording and wave equation inversion for nearsurface material properties: Geophysics, **67**, no. 5, 1602–1611.

de Ridder, S., 2014, Passive seismic surface-wave interferometry for reservoir-scale imaging: PhD thesis, Stanford University.

de Ridder, S. and B. Biondi, 2014, Chaotic wavefield gradiometry: SEP-Report, **155**, 9–16.

de Ridder, S. A. L. and B. L. Biondi, 2015, Near-surface scholte wave velocities at ekofisk from short noise recordings by seismic noise gradiometry: Geophysical Research Letters, **42**, no. 17, 7031–7038.

van Leeuwen, T. and F. J. Herrmann, 2013, Mitigating local minima in full-waveform inversion by expanding the search space: Geophysical Journal International, **195**, no. 1, 661–667.

van Leeuwen T., F. Herrmann, and B. Peters, 2014, A New Take on FWI - Wavefield Reconstruction Inversion: EAGE Technical Program Expanded Abstracts.